



HAL
open science

Microstructure analysis of crust during deep-fat or hot-air frying to understand French fry texture

Têko Gouyo, Éric Rondet, Christian Mestres, Céline Hofleitner, Philippe Bohuon

► To cite this version:

Têko Gouyo, Éric Rondet, Christian Mestres, Céline Hofleitner, Philippe Bohuon. Microstructure analysis of crust during deep-fat or hot-air frying to understand French fry texture. *Journal of Food Engineering*, 2021, 298, pp.110484. 10.1016/j.jfoodeng.2021.110484 . hal-03892001

HAL Id: hal-03892001

<https://institut-agro-montpellier.hal.science/hal-03892001v1>

Submitted on 22 Mar 2023

HAL is a multi-disciplinary open access archive for the deposit and dissemination of scientific research documents, whether they are published or not. The documents may come from teaching and research institutions in France or abroad, or from public or private research centers.

L'archive ouverte pluridisciplinaire **HAL**, est destinée au dépôt et à la diffusion de documents scientifiques de niveau recherche, publiés ou non, émanant des établissements d'enseignement et de recherche français ou étrangers, des laboratoires publics ou privés.



Distributed under a Creative Commons Attribution - NonCommercial 4.0 International License

1 **Microstructure analysis of crust during deep-fat or hot-air frying**
2 **to understand French fry texture.**

3

4 Têko Gouyo ^{a, c}, Eric Rondet ^c, Christian Mestres ^{b, c}, Céline Hofleitner ^a, Philippe Bohuon ^{c*}

5

6 ^aSEB, Ecully Food Science; 112 Chemin du Moulin Carron, 69130 Écully

7

8 ^b CIRAD, UMR QualiSud, Montpellier, France.

9

10 ^c QualiSud, Univ Montpellier, Institut Agro, CIRAD, Univ d'Avignon, Univ de La Réunion,
11 Montpellier, France.

12

13

14 * Corresponding author: Philippe Bohuon, Montpellier SupAgro, UMR QualiSud,

15 1101 av. Agropolis, F-3409 Montpellier, France. Tel. +33 467 87 40 81; Fax: +33 467 61

16 44 44. E-mail address: philippe.bohuon@supagro.fr

17

18

19

20 **Abstract**

21 This study aimed to identify the microstructural parameters of the crust that are
22 responsible for the crispness of French fries. The French fry microstructure was visualized by

23 X-ray micro-computed tomography (XMT). Analysis of the images provided information on
24 the pore size distribution, global porosity of the French fries and local porosity of the crust
25 region. The results revealed that prefrozen French fries do not practically undergo any volume
26 shrinkage during frying. The total porosity created in French fries corresponds to the volume
27 of water loss during frying. The difference between hot-air fried and deep-fat fried French
28 fries was mainly related to the pore diameter and pore size distribution in the crust. Principal
29 component analysis between the sensory and morphometric parameters showed that the
30 volume of small pores (diameter < 0.15 mm) and the span of the pore size distribution in the
31 first millimetres of the crust correlated with the crispness of the product ($r > 0.85$, P value <
32 0.05). Thus, a French fry is crispier if the pores generated in the crust have a small median
33 diameter (diameter < 0.2 mm), as well as a large dispersion of pore diameters.

34 **Highlights (maximum 85 characters)**

- 35 ▶ The French fry crust microstructure revealed by XMT is linked to crispness defined by
36 sensory analysis
- 37 ▶ The total porosity created in pre-frozen French fries corresponds to water loss
- 38 ▶ A higher porosity in the crust generally results in a higher perceived crispness
- 39 ▶ A small pore diameter and heterogeneous pore size distribution in the crust improve
40 the crispness

41 **Keywords**

42 French fries; Crispness; Crust microstructure; X-ray micro-computed tomography, sensory
43 analysis

44 1. Introduction

45 French fries are a specific solid with a moist and soft core and a crispy outer dry crust of
46 approximately 0.5 — 1.5 mm (Bouchon and Aguilera, 2001; Pedreschi and Aguilera, 2002;
47 van Koerten et al., 2015). French fries are popular potato products in many countries because
48 of their attractive texture. Texture is one of the important quality aspects, and a crispy crust is
49 an important factor in the sensory properties of French fries (Vickers and Bourne, 1976;
50 Pedreschi and Aguilera, 2002; Salvador et al., 2009). During potato frying, the formation of
51 the crust is the result of changes in the native potato structure caused by heat and mass
52 transfer (Pedreschi and Aguilera, 2002; Pedreschi, 2009). The structure of the core and crust
53 of a fried product is affected by the time-temperature couple and the frying process, resulting
54 in different types of fried products. The transformations during frying determine the
55 microstructural properties of the crust, such as porosity, pore size shape and pore
56 distribution (Bouchon and Aguilera, 2001; Dalen et al., 2007; Ziiaifar et al., 2010; van
57 Koerten et al., 2015). The microstructure of the crust determines the sensory characteristics of
58 the French fry (Aguilera, 2005; Dalen et al., 2007; van Koerten et al., 2015).

59 In the last decade, hot-air fryers have been developed to overcome the high oil uptake
60 during the frying process with conventional fryers (deep-fat frying). The objective is to reduce
61 fat consumption from French fries. The current disadvantage of this type of fryer is less
62 intense heat and mass transfer, generating French fries with less crispness compared to those
63 obtained by deep-fat frying (Teruel et al., 2015; Gouyo et al., 2020). The most important
64 critical contributors to the physical and rheological behaviour, texture and sensory
65 characteristics of fried food products have sizes in the range of 100 μm (Aguilera, 2005).
66 Knowing how these elements are arranged and interact with the sensory quality of food can
67 contribute to process optimization (Dalen et al., 2007).

68 In the literature, several techniques have been used to study the microstructural changes
69 in food products. These include mercury porosimetry and pycnometry, which represent
70 experimental methods commonly used to quantify the porosity and density of
71 materials (Kassama and Ngadi, 2005; Rahman et al., 2002). Several other techniques have
72 been used, including microscopy (Kaláb et al., 1995; Ferrando and Spiess, 2000; Hesso et al.,
73 2015), magnetic resonance imaging (Horigane et al., 2003; Lucas et al., 2018), computer
74 vision techniques (Hullberg and Ballerini, 2003; Du and Sun, 2006), and most recently, X-ray
75 micro-computed tomography (XMT) (Léonard et al., 2008; Laverse et al., 2011; Adedeji et
76 al., 2011; Hafsa et al., 2014; van Koerten et al., 2015). In XMT, product components are
77 differentiated according to their ability to absorb X-rays, which is directly correlated to their
78 density. The advantage of the latest technique compared to the others is that the XMT is
79 noninvasive, nondestructive and follows a basic sample preparation procedure that does not
80 affect the sample (Adedeji et al., 2011; Alam and Takhar, 2016). The results of XMT analysis
81 provide high-resolution 3D visualization (on the order of a few micrometers according to the
82 apparatus resolution), allowing visualization of the internal morphology of the samples and
83 quantification of the morphometric properties (structure, size, etc.).

84 In recent years, many studies have used XMT to study the internal morphological
85 configuration of many fried food products: deep-fat fried breaded chicken nuggets (Adedeji et
86 al., 2011), deep-fat fried coated chicken nuggets (Adedeji and Ngadi, 2011), deep-fat-fried
87 chicken meat (Kassama and Ngadi, 2005), and bread crumbs (Primo-Martín et al., 2010;
88 Altamirano-Fortoul et al., 2012; Besbes et al., 2013). In the case of French fried potatoes, a
89 few studies have focused on their microstructure. Among them, van Koerten et al. (2015)
90 studied the impact of operating variables (cooking time and temperature) on the structural
91 properties of French fries. In this latest study, the water losses were very low (< 35%) and far
92 from the values that allowed the production of crispy French fries (water loss > 45%

93 according to [Gouyo et al. \(2020\)](#)). Some others, such as [Vauvre et al. \(2014\)](#) and [Alam and](#)
94 [Takhar, \(2016\)](#), have also used XMT to better understand the impact of the microstructure
95 characteristics on the oil uptake during deep-fat frying. (sur des frites? Autre chose? À
96 préciser).

97 The objective of this study was to identify the morphometric parameters of the
98 microstructure of the crust by XMT, which can explain the texture of French fries. Analysis of
99 the images provided information on the pore size distribution, global porosity of the French
100 fries and the gradient porosity of the crust region. A quantitative descriptive analysis was
101 performed to evaluate sensory parameters. An instrumental texture analysis (acoustics and
102 force-deformation test) was also performed. The relationships between the morphometric,
103 sensory and instrumental parameters were established. Finally, this approach was used to
104 compare two products with contrasting textures generated by deep-fat frying and hot-air
105 frying.

106 **2. Materials & Methods**

107 **2.1. Raw materials**

108 The experiments were carried out with frozen French fries (Mc-Cain Tradition, made in
109 Harnes, France, with French potatoes) stored in a cold room at $-18\text{ }^{\circ}\text{C}$ until use. The fries
110 were resized to 60 mm in length and 9 mm in thickness (9×9×60 mm). A specific fry cutter
111 was used to cut the frozen French fries.

112 **2.2. Frying equipment**

113 Two main fryers were used: a commercial deep-fat fryer (Filtra One FF162100 Seb)
114 with a power of 1900 W, a frying capacity of 1.20 kg of French fries and an oil volume of
115 2.10 L and hot-air frying equipment (Airrer Philips XL HD9240/90, Avance Collection,
116 Amsterdam, The Netherlands) with a power of 2100 W and a frying capacity of 1.20 kg of

117 French fries. To determine the amount of moisture evaporated from the potatoes during
118 frying, the fryers were placed on a balance (Sartorius CPA34001S, France, with a capacity of
119 34 kg for 10^{-4} kg of sensibility) that allowed continuous recording of the water loss.

120

121 2.3. Sample preparation

122 The sample preparation aimed to produce samples with different contrasting structures.
123 Each experiment was performed with 0.300 kg of calibrated French fries. Different levels of
124 water loss were obtained ranging from 0% to 60%. The water loss was defined as the mass
125 (kg) or the volume (m^3) of water lost during frying divided by the initial mass (i.m., kg) or the
126 volume (m^3) of the frozen French fries before frying (WL in kg water/kg of fries or m^3 of
127 water/ m^3 of fries). The samples were coded according to their frying conditions, as shown in
128 Table 1. After frying, the middle part of the French fry was cut ($9\times 9\times 30$ mm) and soaked in
129 petroleum ether for 30 seconds to remove most of the oil (this treatment increases the
130 resolution of the XMT images) and then rapidly scanned by XMT. The waiting time from the
131 end of the frying to the XMT analysis was estimated to be an average of 5 to 10 minutes.

132 2.4. XMT scan parameters

133 A volume of $9\times 9\times 30$ mm³ of French fry sample was scanned in a SkyScan 1272
134 (Bruker μ CT, Kontich, Belgium) at a nominal resolution (pixel size) of 11.5 microns
135 employing an aluminium filter 0.25 mm thick. The applied X-ray tube voltage was 42 kV, and
136 the current intensity was 20 μ A. Camera pixel binning of 3×3 was applied. The scan orbit was
137 360 degrees with a rotation step of 0.7 degrees for a scan duration of 23 minutes. The scans
138 were carried out in triplicate with one French fry per test.

139 2.5. Image reconstruction

140 Reconstruction was carried out with a modified Feldkamp ([Feldkamp et al., 1984](#))
141 algorithm using SkyScanTM NRecon software (Version: 1.7.1.0, Bruker μ CT, Kontich,
142 Belgium) accelerated by GPU ([Yan et al., 2008](#)). Gaussian smoothing, ring artefact reduction
143 and beam hardening correction were applied. The reconstruction of each sample produced a
144 series of 845 cross-sections of 896×1344 pixels.

145 2.6. Region of interest selection

146 Region of interest selection, segmentation to binary and morphometric analysis were all
147 performed using SkyScan CT-Analyser (“CTAn”) software (Version: 1.17.7.2, Bruker μ CT,
148 Kontich, Belgium). The "ROI shrink-wrap" function was used to select the region of interest
149 (ROI). This step was used to adjust to the surface or contour line of the fry. The same ROI
150 was analysed for all the samples. It was selected in the center of the reconstructed images to
151 eliminate any edge effects, artefacts and damage from sample cutting. The ROI corresponded
152 to 12 mm of French fries and was composed of 500 stacks (2D images).

153 2.7. Image segmentation to binary and morphometric analysis

154 Global thresholds were selected by the Otsu algorithm ([Otsu, 1979](#)) to segment the
155 image to binary. The same global threshold values were applied to all the measured samples.
156 The 3D morphometric parameters were calculated over the total volume of the French fry and
157 on the crust volume. Noise objects were removed from the binarised image by despeckle
158 morphological operations in CTAn. The porosity was determined as the percentage of voxels
159 segmented as pores to the total number of voxels (void + solid) ([Primo-Martín et al., 2010](#)).
160 The morphometric parameters in 3D were based on the analysis of a marching cubes-type
161 model ([Lorensen and Cline, 1987](#)) with a rendered surface. The pore size in 3D was
162 calculated using the local thickness or “sphere-fitting” (double distance transform) method
163 ([Borgefors, 1996](#); [Hildebrand and Rüegsegger, 1997](#); [Remy and Thiel, 2002](#)). For the crust
164 analysis, a morphological 2D erosion-type operation was performed with a defined radius

165 corresponding to the required crust thickness. Erosions with radii of 43.5, 61 and 87 were
166 used for crust sections with thicknesses of 0.5 mm, 0.7 mm and 1 mm,
167 respectively (Figure 1 b and c). From the pore size distribution, morphometric parameters
168 such as the pore volume (V_p) of different pore sizes ($V_p[0 \text{ to } 0.15 \text{ mm}]$, $V_p[0.15 \text{ to } 0.32 \text{ mm}]$
169 and $V_p[0.32 \text{ to } 0.5 \text{ mm}]$), median diameter (d_{50}) and span = $(d_{90} - d_{10}) / d_{50}$ were estimated.

170 2.8. Sensory analysis

171 The descriptive sensory analysis data of [Gouyo et al., \(2020\)](#) for five samples with
172 contrasting textures (Table 1) were used. Two samples were produced with a conventional
173 deep-fat fryer with water losses of 50 and 60% (i.m.) (DF180_50 and DF180_60,
174 respectively). Three other samples were obtained by hot-air frying at 180 or 200 °C with
175 water losses of 50 and 60% (i.m.) (AY180_50, AY180_60 and AY200_50, respectively).
176 Four sensory descriptors were considered (crispiness of the crust, product hardness, softness
177 of the core and floury of the core).

178 2.9. Instrumental texture analysis

179 The mechanical (penetration test) and acoustic analysis data of [Gouyo et al., \(2020\)](#) for
180 five samples with contrasting textures (Table 1) were also used. The following parameters —
181 maximum force (F_{max} , N) and number of sound peaks (NSP)— were used to characterize the
182 product hardness and crispiness of the crust, respectively.

183 2.10. Statistical analysis

184 The statistical analysis of the results was carried out using XLSTAT version 2017
185 (ANOVA, Student's t-test and PCA test). The ANOVA procedure at a significance level of
186 0.05 and the Tukey test and Student's t-test were applied to assess the significant differences
187 between the investigated parameters. Principal component analysis (PCA) of correlation was
188 also conducted. The sensory and instrumental data were plotted as active variables, and the
189 morphometric data were plotted as supplementary variables.

190 3. Results and discussion

191 3.1. Image description

192 Cross-sectional slices of the XMT scans for different water losses are shown in
193 Figure 2. Overall, the shape of the French fries do not change much. The square section
194 (9×9 mm) is well preserved during frying, but the porosity of the fries increases with
195 increasing water loss. At the end of frying, the French fries have three distinct regions: a
196 peripheral crust, a very porous zone that surrounds the central region, and a core. For the
197 WL = 0% sample, it can be observed that there is already an initial structure with an existing
198 pre-crust that has already formed as a result of the pretreatment of the frozen French fries.
199 This peripheral precrust consists of a single layer of porous bubbles with an approximate
200 diameter of 0.1 mm. Figure 2 also shows that it is difficult to distinguish the boundaries of the
201 crust region. The thickness of the crust differs greatly according to the water loss and also
202 according to the French fry zone considered. For example, for a French fry with
203 WL = 60% (Figure 2 a), the crust thickness of the left part of the image is smaller (0.2 to 0.5
204 mm) than the crust thickness of the right part (0.5 to 1.5 mm). Figure 2b shows that the crust
205 of deep-fat fries is filled with oil (light grey). Despite the soaking of French fries in petroleum
206 ether for 30 seconds, there is still visible oil in the pores of the crust. This residual oil was
207 removed during thresholding. By simple observation, it is difficult to differentiate deep-fat
208 fries from the hot-air fries in Figure 2.

209 3.2. Total porosity and volume change

210 Figure 3 shows the evolution of the total volume and the porosity created in the French
211 fries as a function of water loss for the hot-air and deep-fat fries. The relative uncertainty
212 between replicates is quite low (1.5% to 6%), and there is no significant
213 evolution (P value > 0.05) in the total volume during frying (Figure 2 and Figure 3 a)); the
214 frozen French fries are not subjected to any significant volume shrinkage (< 7%) when

215 dehydrated during frying, even at high water loss (WL = 60%). This is not the case when the
216 raw material is native potatoes. Several studies carried out on frying raw potatoes showed a
217 significant shrinkage of the volume of French fries (30 to 40% of the initial volume) during
218 frying (Krokida et al., 2000; Costa et al., 2001; Yamsaengsung and Moreira, 2002).

219 The total porosity of the French fries was analysed for different water losses. The
220 porosity is defined as the ratio of the cumulative volume of all the pores created relative to the
221 total volume of the analysed French fry (Figure 3 b). The relative uncertainty between
222 replicates is also quite low (2% to 20%), and for the same water loss, the total porosities
223 created in the French fries obtained by deep-fat frying or hot-air frying are not
224 significantly different (P value > 0.05); the porosity created in the fry indeed increases
225 proportional to the water loss of the product independent of the frying condition (hot-air or
226 deep-fat frying). The volume of the water lost during the frying operation corresponds to
227 $92 \pm 15\%$ and $93 \pm 13\%$ of the pore volume created during hot-air frying and deep-fat frying,
228 respectively, thus confirming the lack of volume shrinkage. The measured porosity values are
229 higher than the orders of magnitude mentioned in the literature. For example, for a water loss
230 of 30%, the measured porosity is 28%, whereas Pinthus et al. (1995) obtained 20% and van
231 Koerten et al. (2015) 12% porosity for the same water loss. This can be explained by the
232 significant shrinkage of the French fry in these studies that were performed with raw potatoes,
233 whereas we used frozen French fries.

234 3.3. Porosity of the crust

235 To understand the microstructural phenomena that affect the texture of deep-fat and hot-
236 air French fries, an analysis of the crust zone of French fries was carried out. The main
237 difficulty in the analysis of the crust of the French fry is the delimitation of the geographical
238 zone that corresponds to the crust. Several studies in the literature defined the crust as the
239 superficial porous region (completely dry layer of a fried potato) without defining a specific

240 thickness (Miranda and Aguilera, 2006; Ziiaifar et al., 2010; Lioumbas and Karapantsios,
241 2012a, 2012b; van Koerten et al., 2015). According to these authors, the French fry crust
242 thickness ranged from 0.4 to 1.5 mm. To overcome this problem, the porosity of the French
243 fry crust was determined by peripheral French fry zones at depths of 0-0.2, 0.2-0.5, 0.5-0.7
244 and 0.7-1.0 mm from the French fry surface (Figure 1 b and c). An example of a 0.5 mm thick
245 crust zone analysed is shown in Figure 1 b). When a large and fixed thickness of the crust
246 zone is considered, this may include some empty area, which is located between the crust and
247 the core. This zonal analysis does not provide information on the real thickness of the crust,
248 but it provides information on the microstructure for each crust thickness considered. The
249 microstructure of the selected fry zones is characterised by their porosity and pore size
250 distribution.

251 Figure 4 shows the evolution of the local porosity in different parts of the crust
252 (distances from the potato surface) as a function of water loss. It should be noted (results not
253 shown) that the porosity before frying is 25.53% in the 0 to 0.2 mm zone, 8% between 0.2 and
254 0.5 mm and almost 0% in the more internal zones. It is found that increasing water loss
255 increases the porosity of the crust in any part of the crust. At the beginning of frying, the
256 porosity of the peripheral zone of the crust is more important than that of most internal parts.
257 This is due to the existing porosity in the pre-crust, which has already formed because of the
258 pretreatment of the frozen French fries. This higher porosity in the peripheral area compared
259 to that in the internal zones can be explained by the presence of an evaporation front
260 commonly observed during frying. The same observations were reported by van Koerten et al.
261 (2015). At 25% water loss, the porosities of the different parts of the crust are almost identical
262 ($\epsilon = 35\% - 40\%$). Above 25% water loss, the porosity of the internal parts (0.5 to 1 mm)
263 become significantly higher (P value > 0.5) than that of the peripheral part (0 to 0.2 mm)
264 (Figure 4). In this peripheral part of the crust, the porosity ranges from 35 to 45%, 40 to 50%

265 and 35 to 40% for water losses of 37.5, 50 and 60%, respectively, while the porosity ranges
266 from 55 to 65%, 60 to 78% and 60 to 75% for water losses of 35.5, 50 and 60%, respectively,
267 for part of the inner part of the crust (0.5 to 0.7 mm from the surface). However, regardless of
268 the frying process used, the local porosity in the different parts of the crust is not significantly
269 different (P value > 0.05) for the same water loss. From a water loss of 37.5%, the porosity of
270 the different parts of the crust increase slightly (increases of 5 — 8% and 1 — 5% for water
271 losses of 50% and 60%, respectively). Other authors reported a similar evolution of the crust
272 porosity at the end of frying for different fried foods such as potato strips (Krokida et al.,
273 2000), tortilla chips (Kawas and Moreira, 2001) and sweet potatoes (Taiwo and Baik, 2007).

274 3.4. Pore size distribution in a crust

275 An analysis of morphometric parameters was carried out on the French fry crusts with a
276 thickness of 1 mm. Figure 5 illustrates the evolution of morphometric parameters such as the
277 median diameter (d_{50}) and span in the first millimeter of the French fries (0 to 1 mm) as a
278 function of water loss. The analysis in Figure 5 a) shows that in the first millimeter of the
279 French fries, the median pore diameter of the hot-air fries is larger than that of the deep-fat
280 fries. Beyond 37.5% water loss, this difference in median pore diameter becomes very
281 significant (P value < 0.05); deep-fat frying generates a median pore diameter smaller than 0.2
282 mm in this first millimetre (0 to 1 mm) of the French fry, whereas it is higher than 0.2 mm for
283 hot-air frying. It is also found that the size of the largest pores of the deep-fat fries ranges
284 from 0.15 mm to 0.5 mm for 50% water loss and from 0.18 mm to 0.6 mm for 60% water
285 loss. For the same water losses, the largest pore sizes of the hot-air fries range from 0.3 mm to
286 0.7 mm and 0.4 mm to 0.8 mm, respectively. For the same total porosity created in the crust
287 (figure 4), the pore size distribution depends on the frying process. In figure 5 b), the span
288 evolution is plotted as a function of water loss. The span of the deep-fat fries decreases
289 slightly from 3 to 2.5 as the water loss increases, whereas for the hot-air fries, the span in the

290 first millimeter decreases significantly (P value < 0.05) from approximately 3 to 1.5 as the
291 water loss increases. For French fries with a water loss greater than 37.5%, the span of the
292 deep-fat fries is significantly (P value < 0.05) higher than that of the hot-air fries. The pore
293 size distribution of the deep-fat fries is therefore more heterogeneous than that of the hot-air
294 fries for the same water loss. Deep-fat frying generates smaller pore diameters and a
295 heterogeneous pore size distribution in the first millimeter of the crust, while hot-air frying
296 generates larger pores and a more homogeneous pore size distribution. However, it is
297 important to note that the difference in the pore diameter distribution ($V_p[0 \text{ to } 0.15 \text{ mm}]$,
298 d_{50} and span) observed between the hot-air fries and deep-fat fries decreases when the crust
299 thickness considered is lower (0.7 mm or 0.5 mm).

300 3.5. Local distribution of pore sizes

301 The pore size distribution was obtained by measuring the pore sizes in the volume of
302 interest of 500 stacks of French fry crusts (Figure 1). Figure 6 shows the cumulative
303 percentages of the pore size distributions in different parts of the crusts of hot-air fries and
304 deep-fat fries. The pore diameter globally increases from the surface to the core of the fry for
305 the same water loss. The first 0.2 mm of the crust of the hot-air and deep-fat fries have small
306 pore diameters (for WL= 50%, $d_{50} = 0.08 \text{ mm}$ and for WL= 60%, $d_{50} = 0.05 \text{ mm}$) compared
307 to the deeper parts of the crust. [Vauvre et al. \(2014\)](#) also found that pore diameter increased
308 moving away from the surface of the fry. The median diameter of the pore in the crust from
309 0.5 to 0.7 mm of the surface increases with water loss, while the median pore diameter in the
310 crust from 0 to 0.2 mm does not change significantly. The structure of this peripheral part
311 does not appear to evolve as a function of water loss.

312 Through comparison of the pore size distributions of the hot-air fries and deep-fat fries
313 for the same water loss (Figure 6), it is found that the pore size of the hot-air fries is larger
314 than that of deep-fat fries in the different parts of the crust except for the first 0.2 mm. For

315 example, for deep-fat fries with water loss of 50%, the median pore sizes in the different parts
316 of the crust (0 to 0.2, 0.2 to 0.5, 0.5 to 0.7 and 0.7 to 1 mm) are 0.08, 0.1, 0.3 and 0.5 mm,
317 respectively. For hot-air fries with the same water loss (50%), the pore diameter varies in the
318 different parts of the crust from 0.09, 0.18, 0.38 and 0.6, respectively. The difference between
319 the pore diameters of the hot-air fries and deep-fat fries is not significant (P value > 0.5) in the
320 first 0.2 mm of the crust. Nevertheless, it is significantly (P value < 0.5) higher in the deeper
321 parts of the crust. The difference in the frequency of the pore diameter distribution between
322 the hot-air fries and deep-fat fries may be associated with transfer phenomena in the French
323 fries during frying. In fact, deep-fat frying is a process of heat and water transfer that causes
324 fast water evaporation from food. In contrast to deep-fat frying, hot-air frying induces a lower
325 heat and mass transfer with a heat transfer coefficient $h < 100 \text{ W.m}^{-2} \cdot \text{K}^{-1}$ and an evaporation
326 flux density $< 4 \cdot 10^{-3} \text{ kg.m}^{-2} \cdot \text{s}^{-1}$ (Andrés et al., 2013; Teruel et al., 2015). The high heat and
327 mass transfer intensity in deep-fat frying ($150 < h < 1500 \text{ W.m}^{-2} \cdot \text{K}^{-1}$ and an evaporation flux
328 density $> 5 \cdot 10^{-3} \text{ kg.m}^{-2} \cdot \text{s}^{-1}$) (Costa et al., 1999; Vitrac et al., 2002; Vitrac and Trystram, 2005)
329 lead to faster dehydration of the surface of the fry, which becomes rigid and can oppose the
330 water evaporation fluxes. This generates an overpressure that can reach 30 kPa in French fries
331 during deep-fat frying (Li et al., 2011; Patsioura et al., 2016; Vauvre et al., 2014). A high
332 intensity of transfers can therefore generate high pressure on the structure of the potatoes and
333 create a high number of small-sized pores in the crust. Van Koerten et al. (2015) also showed
334 that the higher transfer intensity permitted a larger evaporation zone inside French fries and
335 allowed the creation of a higher number of small-sized pores but also a very heterogeneous
336 pore size distribution. On the other hand, the lower intensity of heat and water transfer in the
337 case of hot-air frying could lead to a slower creation of new pores and be more favourable to
338 the growth of the first pores created. Overpressure data are not available in the literature, but
339 this parameter can be expected to be lower for hot-air frying. Van Loon (2005) indicated that

340 the low overpressure induced by hot-air frying was insufficient to cause the cell separation
341 necessary for a more distributed porosity.

342 3.6. Morphometric parameters *versus* sensory and instrumental textures

343 The samples in Table 1 marked with an asterisk * were characterized by sensory and
344 instrumental texture analysis; the data were obtained from the research of [Gouyo et al. \(2020\)](#)
345 (crispiness of the crust, product hardness, softness of the core and flouriness of the core). The
346 data show that the deep-fat fries were crispier than the hot-air fries, and those with 60% water
347 loss (BH180_60) were the crispiest of all the samples. The data showed that the acoustic
348 parameter NSP (number of sound peaks) ($r = 0.89$; $P\text{-value} < 0.01$) was strongly positively
349 correlated with the crispness of the crust and that the mechanical (penetration test) parameter
350 F_{\max} (maximum force) was strongly correlated with the product hardness ($r = 0.9$;
351 $P\text{ value} < 0.01$). In Figure 7, a relationship is established between the morphometric
352 parameters of the first millimeter of the crust of the French fries and the sensory
353 descriptors and instrumental texture parameters by principal component analysis (PCA). The
354 PCA shows that 96.90% of the variability could be explained by the first two main
355 components: 58.25% by the first component F1 and 38.65% by the second component F2.
356 The morphometric parameters are projected as supplementary variables and do not influence
357 the principal components of the analysis. The first dimension (F1 axis) is built by the
358 contributions of the following variables: product hardness (28.06%), softness of the
359 core (23.91%), floury of the core (20.30%) and F_{\max} (24.58%), which are highly correlated
360 with this axis ($|r| > 0.84$). The second axis (F2 axis) is built by the crispiness of the
361 crust (43.03) and the NSP (38.13), which are very highly correlated with this axis ($r > 0.94$).
362 The bi-plot (Figure 7) indeed illustrates that deep-fat fried products (DF180_60 and
363 DF180_50) are associated with the highest values of the sensory crispiness of the crust and of
364 the NSP. The crispiness of the crust and NSP are indeed strongly positively correlated, with a

365 correlation coefficient $r = 0.94$ (P value < 0.05). On the first axis, the hot-air fried product
366 with 60% water loss (AY180_60), which was considered the hardest and not crispy by [Gouyo](#)
367 [et al. \(2020\)](#), is related to higher values of product hardness, floury of the core and F_{max} .

368 The span of the pore size distribution and the volume of pores with low diameters ($V_p[0$
369 $\text{to } 0.15]$ and $V_p[0.32 \text{ to } 0.5]$) appear highly and positively correlated with axis 2 ($r = 0.84,$
370 0.87 and 0.86 , respectively), while d_{50} and the volume of the large pores are negatively
371 correlated with this axis ($r = -0.71$ and -0.87 , respectively). The crispiness of the crust thus
372 increases when small pores are formed but decrease when large pores are formed; the
373 crispness of the crust and NSP are indeed significantly (P value < 0.05) positively correlated
374 to the span and the volume of pores with diameters ranging from 0 to 0.15 mm. These
375 correlations do not appear, however, to be linear (Figure 8). The median diameter (d_{50}) is
376 poorly (P value < 0.10) anti-correlated with the crispiness of the crust, but the regression
377 appears to be more linear. This relationship between small pores and crispness corresponds to
378 what is expected because according to [Vincent, \(1998\)](#), [Thanatuksorn et al. \(2007\)](#) and [Gouyo](#)
379 [et al. \(2020\)](#), a high number of force peaks and sound peaks (NSP) corresponds to a higher
380 fracturability of the crust. These peaks basically represent numerous small fracture incidents
381 during deformation ([van Koerten et al., 2015](#)). It is therefore considered that the more small
382 pores are present in the first millimetre (0 to 1 mm) of a French fry instead of large pores, the
383 more small incidents of fracture occur during deformation of the French fry.

384 For axis 1, the total porosity (ϵ) appears positively correlated with this axis and with the
385 floury of the core ($r = 0.88$, P value < 0.05). As the porosity increases, the floury of the core
386 increases. This could be explained by the fact that a high-water loss of the product leads to a
387 very porous product and a very dry core that gives the sensation of flouriness.

388 These results showed that the increase in the span of the pore size distribution and the
389 volume of the pores with diameters ranging from 0 to 0.15 mm ($V_p[0 \text{ to } 0.15]$) and the

390 decrease in the d_{50} are favourable to a good crispness of the fried product. The results show
391 that crispness is not the consequence of a single morphometric parameter but a combination
392 of microstructures generated in the crust. To have a good level of crispness in fried products,
393 heterogeneous pore sizes with median diameters smaller than 0.2 mm must therefore be
394 generated in the first millimetre of the product crust.

395 **4. Conclusion**

396 The microstructure development of the crust of French fries obtained by hot-air and
397 deep-fat frying was analysed with XMT. The results showed that the prefrozen French fries
398 do not practically undergo any volume shrinkage during frying (deep-fat or hot-air frying). It
399 is shown that the total porosity created in French fries is proportional to the water loss during
400 frying, regardless of the frying process. The French fries obtained by hot-air frying mainly
401 differ from those obtained by deep-fat frying through a larger mean pore diameter. Principal
402 component analysis (PCA) between the sensory, instrumental and morphometric parameters
403 of the first millimeter of the French fry correlates the microstructure of the crust developed
404 during frying with the crispness of the crust. To have a good level of crispness in fried
405 products, the frying process must generate heterogeneous pores with a high volume of pores
406 with diameters ranging from 0 to 0.15 mm and median diameter smaller than 0.2 mm in the
407 first millimetre of the crust.

408

409

410

411

412

413

414

415
416
417
418
419
420

Table 1: French fry sample conditions obtained by deep fat frying (DF) or air frying (AY) at two different temperatures (for oil bath or air) and six different water loss levels.

Sample code	Frying equipment	T °C	Water loss (% i.m.)
DF180_5	Deep-Fat Fryer	180	5.0
DF180_12.5	Deep-Fat Fryer	180	12.5
DF180_25	Deep-Fat Fryer	180	25.0
DF180_37.5	Deep-Fat Fryer	180	37.5
DF180_50 *	Deep-Fat Fryer	180	50.0
DF180_60 *	Deep-Fat Fryer	180	60.0
AY180_5	Air Fryer	180	5.0
AY180_12.5	Air Fryer	180	12.5
AY180_25	Air Fryer	180	25.0
AY180_37.5	Air Fryer	180	37.5
AY180_50 *	Air Fryer	180	50.0
AY180_60 *	Air Fryer	180	60.0
AY200_50 *	Air Fryer	200	50.0

421
422
423
424
425
426
427
428
429

Samples marked with an asterisk (*) correspond to samples used for sensory analysis according to the data from [Gouyo et al. \(2020\)](#). i.m. corresponds to the initial mass.

430 5. Acknowledgements

431 This study was funded by SEB Group, ANRT “Agence National de la Recherche et de la
432 Technologie” and CIRAD-Montpellier. We would like to express our thanks to Léa Ollier,
433 Laboratory Technician at QualiSud UMR, for his assistance.

434 6. References

- 435 Adedeji, A.A., Liu, L., Ngadi, M.O., 2011. Microstructural evaluation of deep-fat fried
436 chicken nugget batter coating using confocal laser scanning microscopy. *J. Food Eng.*
437 102, 49–57. <https://doi.org/10.1016/j.jfoodeng.2010.08.002>
- 438 Adedeji, A.A., Ngadi, M.O., 2011. Microstructural Characterization of Deep-Fat Fried
439 Breaded Chicken Nuggets Using X-Ray Micro-Computed Tomography. *J. Food*
440 *Process Eng.* 34, 2205–2219. <https://doi.org/10.1111/j.1745-4530.2009.00565.x>
- 441 Aguilera, J.M., 2005. Why food microstructure? *J. Food Eng., IV Iberoamerican Congress of*
442 *Food Engineering (CIBIA IV)* 67, 3–11.
443 <https://doi.org/10.1016/j.jfoodeng.2004.05.050>
- 444 Alam, T., Takhar, P.S., 2016. Microstructural Characterization of Fried Potato Disks Using
445 X-Ray Micro Computed Tomography. *J. Food Sci.* 81, E651–E664.
446 <https://doi.org/10.1111/1750-3841.13219>
- 447 Altamirano-Fortoul, R., Le-Bail, A., Chevallier, S., Rosell, C.M., 2012. Effect of the amount
448 of steam during baking on bread crust features and water diffusion. *J. Food Eng.* 108,
449 128–134. <https://doi.org/10.1016/j.jfoodeng.2011.07.015>
- 450 Andrés, A., Arguelles, Á., Castelló, M.L., Heredia, A., 2013. Mass Transfer and Volume
451 Changes in French Fries During Air Frying. *Food Bioprocess Technol.* 6, 1917–1924.
452 <https://doi.org/10.1007/s11947-012-0861-2>
- 453 Besbes, E., Jury, V., Monteau, J.-Y., Le Bail, A., 2013. Characterizing the cellular structure of
454 bread crumb and crust as affected by heating rate using X-ray microtomography. *J.*
455 *Food Eng.* 115, 415–423. <https://doi.org/10.1016/j.jfoodeng.2012.10.005>
- 456 Borgefors, G., 1996. On Digital Distance Transforms in Three Dimensions. *Comput. Vis.*
457 *Image Underst.* 64, 368–376. <https://doi.org/10.1006/cviu.1996.0065>
- 458 Bouchon, P., Aguilera, J.M., 2001. Microstructural analysis of frying potatoes. *Int. J. Food*
459 *Sci. Technol.* 36, 669–676. <https://doi.org/10.1046/j.1365-2621.2001.00499.x>

- 460 Costa, R.M., Oliveira, F.A.R., Boutcheva, G., 2001. Structural changes and shrinkage of
461 potato during frying. *Int. J. Food Sci. Technol.* 36, 11–23.
462 <https://doi.org/10.1046/j.1365-2621.2001.00413.x>
- 463 Costa, R.M., Oliveira, F.A.R., Delaney, O., Gekas, V., 1999. Analysis of the heat transfer
464 coefficient during potato frying. *J. Food Eng.* 39, 293–299.
465 [https://doi.org/10.1016/S0260-8774\(98\)00169-1](https://doi.org/10.1016/S0260-8774(98)00169-1)
- 466 Dalen, G.V., Nootenboom, P., Vliet, L.J.V., Voortman, L., Esveld, E., 2007. 3-D imaging,
467 analysis and modelling of porous cereal products using x-ray microtomography. *Image*
468 *Anal. Stereol.* 26, 169–177. <https://doi.org/10.5566/ias.v26.p169-177>
- 469 Du, C.-J., Sun, D.-W., 2006. Automatic measurement of pores and porosity in pork ham and
470 their correlations with processing time, water content and texture. *Meat Sci.* 72, 294–
471 302. <https://doi.org/10.1016/j.meatsci.2005.07.016>
- 472 Feldkamp, L.A., Davis, L.C., Kress, J.W., 1984. Practical cone-beam algorithm. *JOSA A* 1,
473 612–619. <https://doi.org/10.1364/JOSAA.1.000612>
- 474 Ferrando, M., Spiess, W.E.L., 2000. Review: Confocal scanning laser microscopy. A
475 powerful tool in food science. *Food Sci. Technol. Int.* 6, 267–284.
476 <https://doi.org/10.1177/108201320000600402>
- 477 Gouyo, T., Mestres, C., Maraval, I., Fontez, B., Hofleitner, C., Bohuon, P., 2020. Assessment
478 of acoustic-mechanical measurements for texture of French fries: Comparison of deep-
479 fat frying and air frying. *Food Res. Int.* 131, 108947.
480 <https://doi.org/10.1016/j.foodres.2019.108947>
- 481 Hafsa, I., Cuq, B., Kim, S.J., Le Bail, A., Ruiz, T., Chevallier, S., 2014. Description of
482 internal microstructure of agglomerated cereal powders using X-ray microtomography
483 to study of process–structure relationships. *Powder Technol.* 256, 512–521.
484 <https://doi.org/10.1016/j.powtec.2014.01.073>
- 485 Hesso, N., Garnier, C., Loisel, C., Chevallier, S., Bouchet, B., Le-Bail, A., 2015. Formulation
486 effect study on batter and cake microstructure: Correlation with rheology and texture.
487 *Food Struct.* 5, 31–41. <https://doi.org/10.1016/j.foostr.2015.03.002>
- 488 Hildebrand, T., Rügsegger, P., 1997. A new method for the model-independent assessment
489 of thickness in three-dimensional images. *J. Microsc.* 185, 67–75.
490 <https://doi.org/10.1046/j.1365-2818.1997.1340694.x>
- 491 Horigane, A.K., Motoi, H., Irie, K., Yoshida, M., 2003. Observation of the Structure,
492 Moisture Distribution, and Oil Distribution in the Coating of Tempura by NMR Micro

493 Imaging. *J. Food Sci.* 68, 2034–2039. <https://doi.org/10.1111/j.1365->
494 [2621.2003.tb07014.x](https://doi.org/10.1111/j.1365-2621.2003.tb07014.x)

495 Hullberg, A., Ballerini, L., 2003. Pore formation in cured-smoked pork determined with
496 image analysis - effects of tumbling and RN- gene. *Meat Sci.* 65, 1231–1236.
497 [https://doi.org/10.1016/S0309-1740\(03\)00030-5](https://doi.org/10.1016/S0309-1740(03)00030-5)

498 Kaláb, M., Allan-Wojtas, P., Miller, S.S., 1995. Microscopy and other imaging techniques in
499 food structure analysis. *Trends Food Sci. Technol.* 6, 177–186.
500 [https://doi.org/10.1016/S0924-2244\(00\)89052-4](https://doi.org/10.1016/S0924-2244(00)89052-4)

501 Kassama, L.S., Ngadi, M.O., 2005. Pore structure characterization of deep-fat-fried chicken
502 meat. *J. Food Eng.* 66, 369–375. <https://doi.org/10.1016/j.jfoodeng.2004.04.003>

503 Kawas, M.L., Moreira, R.G., 2001. Effect of Degree of Starch Gelatinization on Quality
504 Attributes of Fried Tortilla Chips. *J. Food Sci.* 66, 300–306.
505 <https://doi.org/10.1111/j.1365-2621.2001.tb11336.x>

506 Krokida, M.K., Oreopoulou, V., Maroulis, Z.B., 2000. Effect of frying conditions on
507 shrinkage and porosity of fried potatoes. *J. Food Eng.* 43, 147–154.
508 [https://doi.org/10.1016/S0260-8774\(99\)00143-0](https://doi.org/10.1016/S0260-8774(99)00143-0)

509 Laverse, J., Mastromatteo, M., Frisullo, P., Del Nobile, M.A., 2011. X-ray microtomography
510 to study the microstructure of cream cheese-type products. *J. Dairy Sci.* 94, 43–50.
511 <https://doi.org/10.3168/jds.2010-3524>

512 Léonard, A., Blacher, S., Nimmol, C., Devahastin, S., 2008. Effect of far-infrared radiation
513 assisted drying on microstructure of banana slices: An illustrative use of X-ray
514 microtomography in microstructural evaluation of a food product. *J. Food Eng.* 85,
515 154–162. <https://doi.org/10.1016/j.jfoodeng.2007.07.017>

516 Li, Y., Mason, G., Morrow, N.R., Ruth, D.W., 2011. Capillary Pressure at a Saturation Front
517 During Restricted Counter-Current Spontaneous Imbibition with Liquid Displacing
518 Air. *Transp. Porous Media* 87, 275–289. <https://doi.org/10.1007/s11242-010-9681-x>

519 Lioumbas, J.S., Karapantsios, T.D., 2012a. Effect of Potato Orientation on Evaporation Front
520 Propagation and Crust Thickness Evolution during Deep-Fat Frying. *J. Food Sci.* 77,
521 E297–E305. <https://doi.org/10.1111/j.1750-3841.2012.02915.x>

522 Lioumbas, J.S., Karapantsios, T.D., 2012b. Evaporation Front Compared with Crust
523 Thickness in Potato Deep-Fat Frying. *J. Food Sci.* 77, E17–E25.
524 <https://doi.org/10.1111/j.1750-3841.2011.02472.x>

525 Lorensen, W.E., Cline, H.E., 1987. Marching cubes: A high resolution 3D surface
526 construction algorithm. *ACM SIGGRAPH Comput. Graph.* 21, 163–169.
527 <https://doi.org/10.1145/37402.37422>

528 Lucas, T., Collewet, G., Bousquière, J., Deligny, C., 2018. The size of eye-shaped bubbles in
529 Danish pastry in relation to the size of fat fragments; A reverse engineering approach
530 of the alveolar structure. *J. Food Eng.* 237, 194–203.
531 <https://doi.org/10.1016/j.jfoodeng.2018.04.025>

532 Miranda, M.L., Aguilera, J.M., 2006. Structure and Texture Properties of Fried Potato
533 Products. *Food Rev. Int.* 22, 173–201. <https://doi.org/10.1080/87559120600574584>

534 Otsu, N., 1979. A Threshold Selection Method from Gray-Level Histograms. *IEEE Trans.*
535 *Syst. Man Cybern.* 9, 62–66. <https://doi.org/10.1109/TSMC.1979.4310076>

536 Patsioura, A., Vauvre, J.-M., Kesteloot, R., Smith, P., Trystram, G., Vitrac, O., 2016. Chapter
537 17 - Mechanisms of Oil Uptake in French Fries, in: Singh, J., Kaur, L. (Eds.),
538 *Advances in Potato Chemistry and Technology (Second Edition)*. Academic Press,
539 San Diego, pp. 503–526. <https://doi.org/10.1016/B978-0-12-800002-1.00017-0>

540 Pedreschi, F., 2009. Fried and Dehydrated Potato Products. pp. 319–337.
541 <https://doi.org/10.1016/B978-0-12-374349-7.00011-8>

542 Pedreschi, F., Aguilera, J.M., 2002. Some Changes in Potato Chips During Frying Observed
543 by Confocal Laser Scanning Microscopy (CLSM). *Food Sci. Technol. Int.* 8, 197–201.
544 <https://doi.org/10.1106/108201302027931>

545 Pinthus, E.J., Weinberg, P., Saguy, I.S., 1995. Deep-Fat Fried Potato Product Oil Uptake as
546 Affected by Crust Physical Properties. *J. Food Sci.* 60, 770–772.
547 <https://doi.org/10.1111/j.1365-2621.1995.tb06225.x>

548 Primo-Martín, C., van Dalen, G., Meinders, M.B.J., Don, A., Hamer, R.H., van Vliet, T.,
549 2010. Bread crispness and morphology can be controlled by proving conditions. *Food*
550 *Res. Int.* 43, 207–217. <https://doi.org/10.1016/j.foodres.2009.09.030>

551 Rahman, M.S., Al-Amri, O.S., Al-Bulushi, I.M., 2002. Pores and physico-chemical
552 characteristics of dried tuna produced by different methods of drying. *J. Food Eng.* 53,
553 301–313. [https://doi.org/10.1016/S0260-8774\(01\)00169-8](https://doi.org/10.1016/S0260-8774(01)00169-8)

554 Remy, E., Thiel, E., 2002. Medial axis for chamfer distances: computing look-up tables and
555 neighbourhoods in 2D or 3D. *Pattern Recognit. Lett., Discrete Geometry for Computer*
556 *Imagery* 23, 649–661. [https://doi.org/10.1016/S0167-8655\(01\)00141-6](https://doi.org/10.1016/S0167-8655(01)00141-6)

557 Salvador, A., Varela, P., Sanz, T., Fiszman, S.M., 2009. Understanding potato chips crispy
558 texture by simultaneous fracture and acoustic measurements, and sensory analysis.
559 LWT - Food Sci. Technol. 42, 763–767. <https://doi.org/10.1016/j.lwt.2008.09.016>

560 Taiwo, K.A., Baik, O.D., 2007. Effects of pre-treatments on the shrinkage and textural
561 properties of fried sweet potatoes. LWT - Food Sci. Technol. 40, 661–668.
562 <https://doi.org/10.1016/j.lwt.2006.03.005>

563 Teruel, M. del R., Gordon, M., Linares, M.B., Garrido, M.D., Ahromrit, A., Niranjana, K.,
564 2015. A Comparative Study of the Characteristics of French Fries Produced by Deep
565 Fat Frying and Air Frying. J. Food Sci. 80, E349–E358. <https://doi.org/10.1111/1750-3841.12753>

567 Thanatuksorn, P., Kajiwaru, K., Suzuki, T., 2007. Characterization of deep-fat frying in a
568 wheat flour–water mixture model using a state diagram. J. Sci. Food Agric. 87, 2648–
569 2656. <https://doi.org/10.1002/jsfa.3027>

570 van Koerten, K.N., Schutyser, M.A.I., Somsen, D., Boom, R.M., 2015. Crust morphology and
571 crispness development during deep-fat frying of potato. Food Res. Int. 78, 336–342.
572 <https://doi.org/10.1016/j.foodres.2015.09.022>

573 Vauvre, J.-M., Kesteloot, R., Patsioura, A., Vitrac, O., 2014. Microscopic oil uptake
574 mechanisms in fried products. Eur. J. Lipid Sci. Technol. 116, 741–755.
575 <https://doi.org/10.1002/ejlt.201300278>

576 Vickers, Z., Bourne, M.C., 1976. Crispness in Foods—a Review. J. Food Sci. 41, 1153–1157.
577 <https://doi.org/10.1111/j.1365-2621.1976.tb14406.x>

578 Vincent, J.F.V., 1998. The quantification of crispness. J. Sci. Food Agric. 78, 162–168.
579 [https://doi.org/10.1002/\(SICI\)1097-0010\(199810\)78:2<162::AID-JSFA97>3.0.CO;2-3](https://doi.org/10.1002/(SICI)1097-0010(199810)78:2<162::AID-JSFA97>3.0.CO;2-3)

580 Vitrac, O., Dufour, D., Trystram, G., Raoult-Wack, A.-L., 2002. Characterization of heat and
581 mass transfer during deep-fat frying and its effect on cassava chip quality. J. Food
582 Eng. 53, 161–176. [https://doi.org/10.1016/S0260-8774\(01\)00153-4](https://doi.org/10.1016/S0260-8774(01)00153-4)

583 Vitrac, O., Trystram, G., 2005. A method for time and spatially resolved measurement of
584 convective heat transfer coefficient (h) in complex flows. Chem. Eng. Sci. 60, 1219–
585 1236. <https://doi.org/10.1016/j.ces.2004.09.046>

586 Yamsaengsung, R., Moreira, R.G., 2002. Modeling the transport phenomena and structural
587 changes during deep fat frying: Part I: model development. J. Food Eng. 53, 1–10.
588 [https://doi.org/10.1016/S0260-8774\(01\)00134-0](https://doi.org/10.1016/S0260-8774(01)00134-0)

589 Yan, G., Tian, J., Zhu, S., Dai, Y., Qin, C., 2008. Fast cone-beam CT image reconstruction
590 using GPU hardware. J. X-Ray Sci. Technol. 16, 225–234.

591 Ziaifar, A.M., Courtois, F., Trystram, G., 2010. Porosity Development and Its Effect on Oil
592 Uptake During Frying Process. *J. Food Process Eng.* 33, 191–212.
593 <https://doi.org/10.1111/j.1745-4530.2008.00267.x>
594

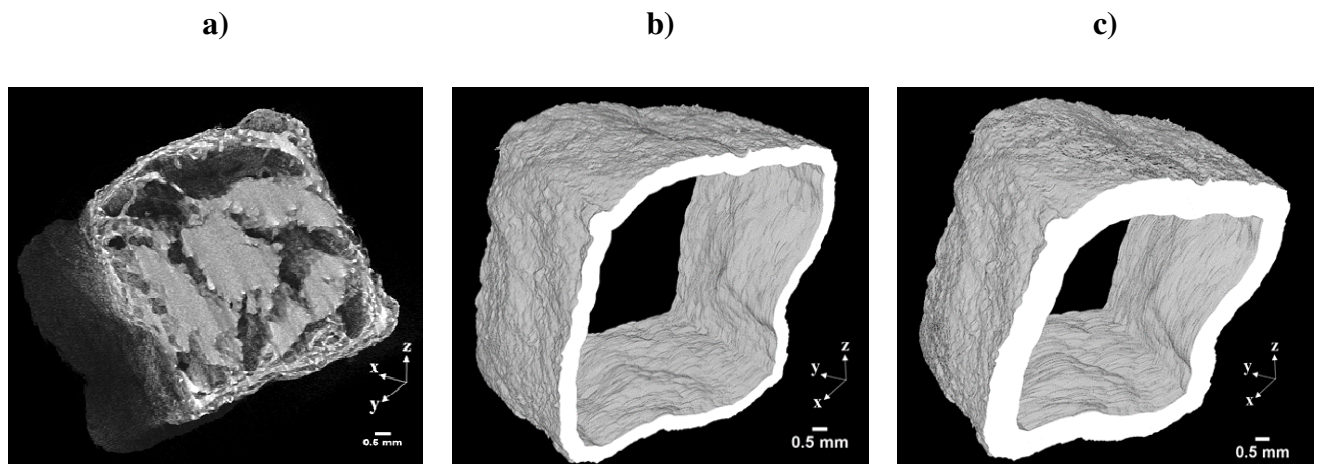


Figure 1: 3D image of a) the global French fry obtained from XMT of hot-air frying and French fry with an ROI corresponding to crusts b) 0.5 mm thick and c) 1 mm thick.

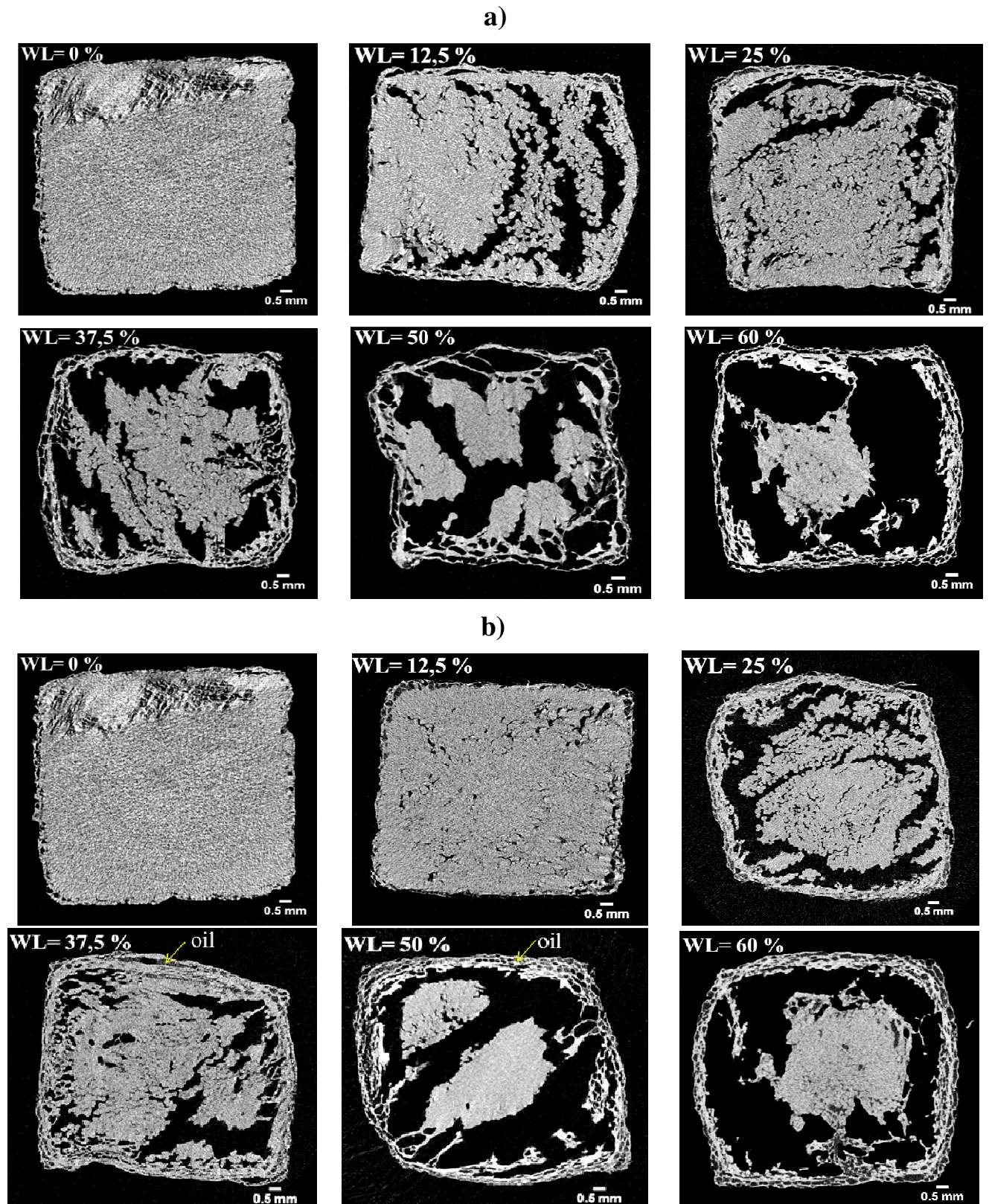


Figure 1: Cross-sectional slices (2D images) obtained from X-ray micro-computed tomography of **a)** hot-air fries and **b)** deep-fat fries as a function of water loss (WL) expressed in kg of water per kg of initial mass.

The square section was preserved during frying, and the porosity of the fries increased with increasing water loss.

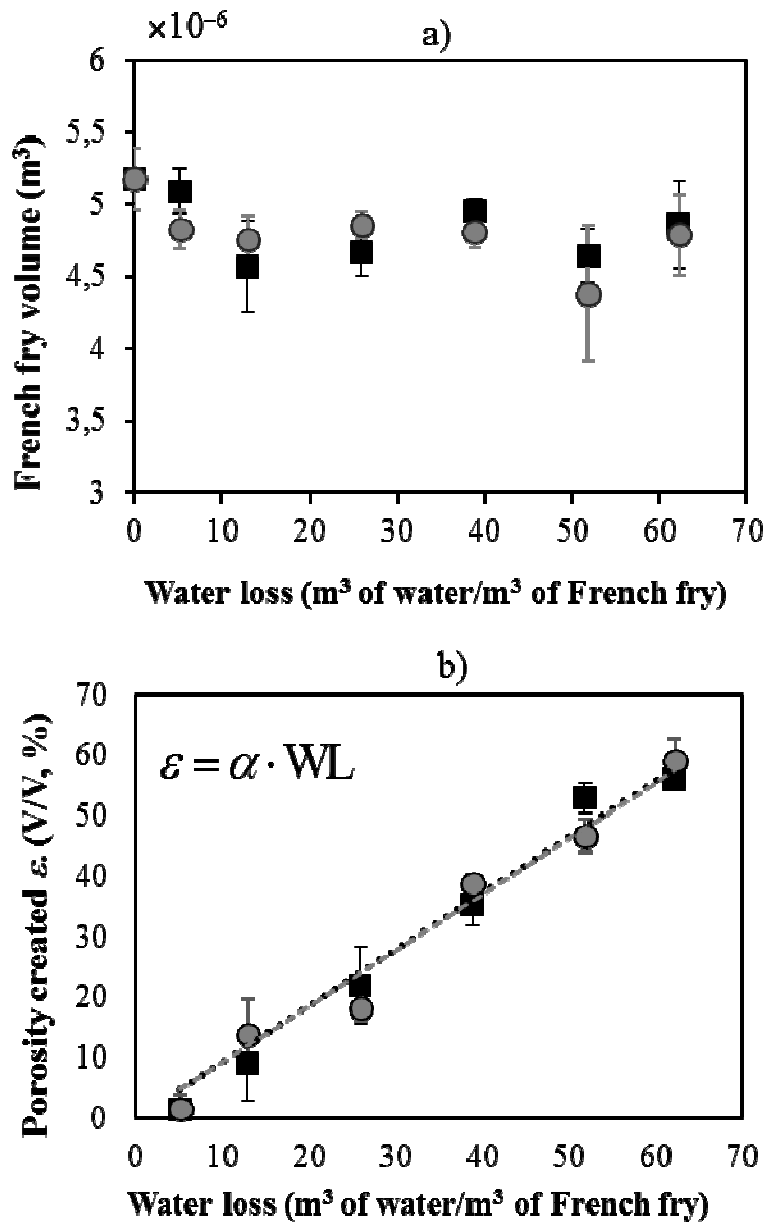


Figure 1: a) Volume change in hot-air frying (●) and deep-fat frying (■) and b) total porosity created (ϵ) as a function of water loss (WL). The dashed line represents the linear regression of hot-air frying ($\alpha = 0.92 \pm 0.15$ with $R^2 = 0.98$) and deep-fat frying ($\alpha = 0.93 \pm 0.13$ with $R^2 = 0.98$). Error bars represent the standard deviation between replicates.

Figure 3a highlights a low volume shrinkage of French fries during frying. The porosity created in the fry increases proportionally to the water loss and independently of the frying conditions (Figure 3 b).

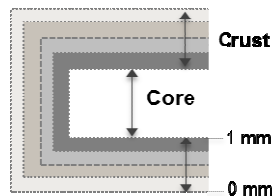
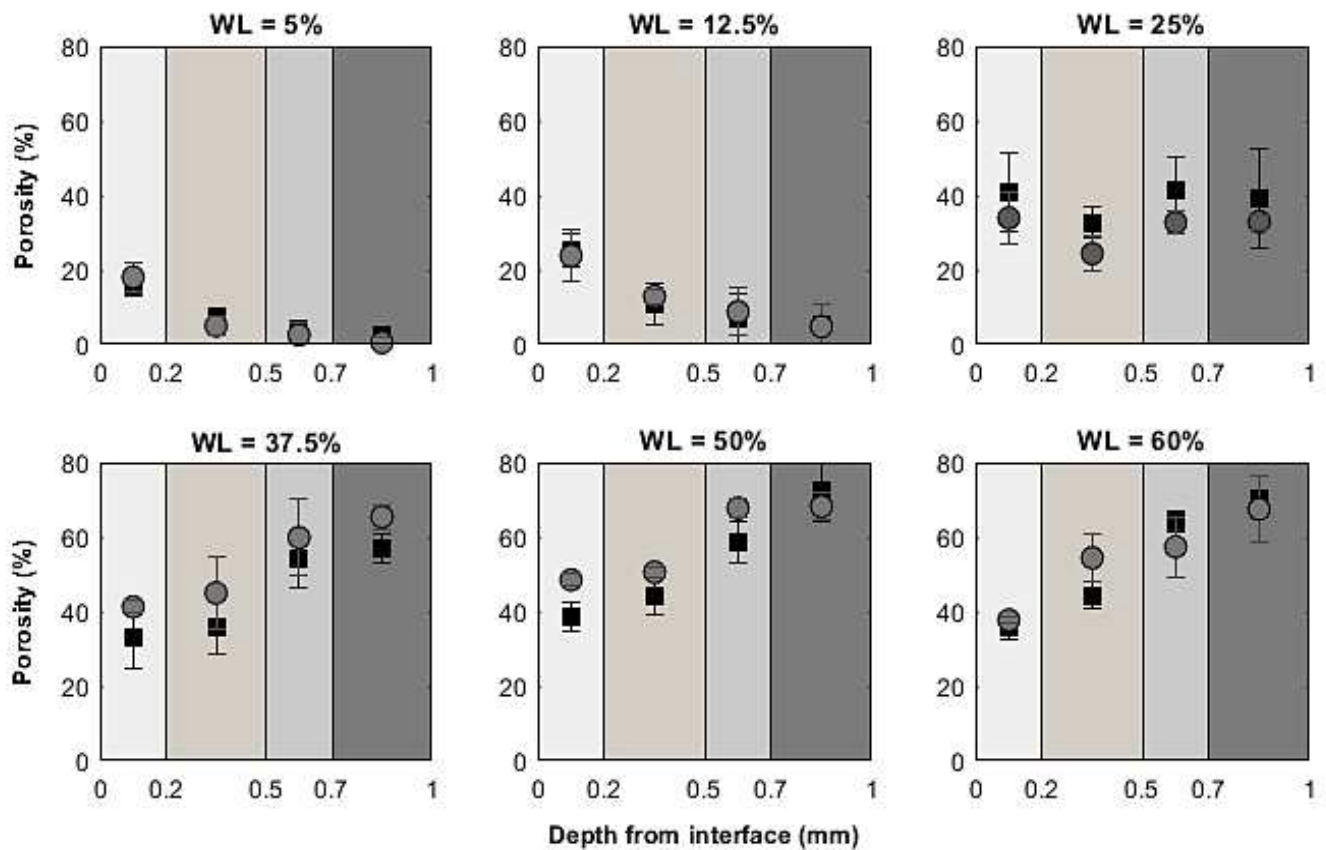


Figure 1: Evolution of the local porosity created in different parts of the crust as a function of water loss (WL) for hot-air French fries (●) and deep-fat French fries (■). Error bars represent the standard deviation between replicates.

Increasing water loss increases the porosity of the crust in any part of the crust. In each part of the crust, the local porosity created by the two types of frying process was not significantly different (P value > 0.05) for the same water loss.

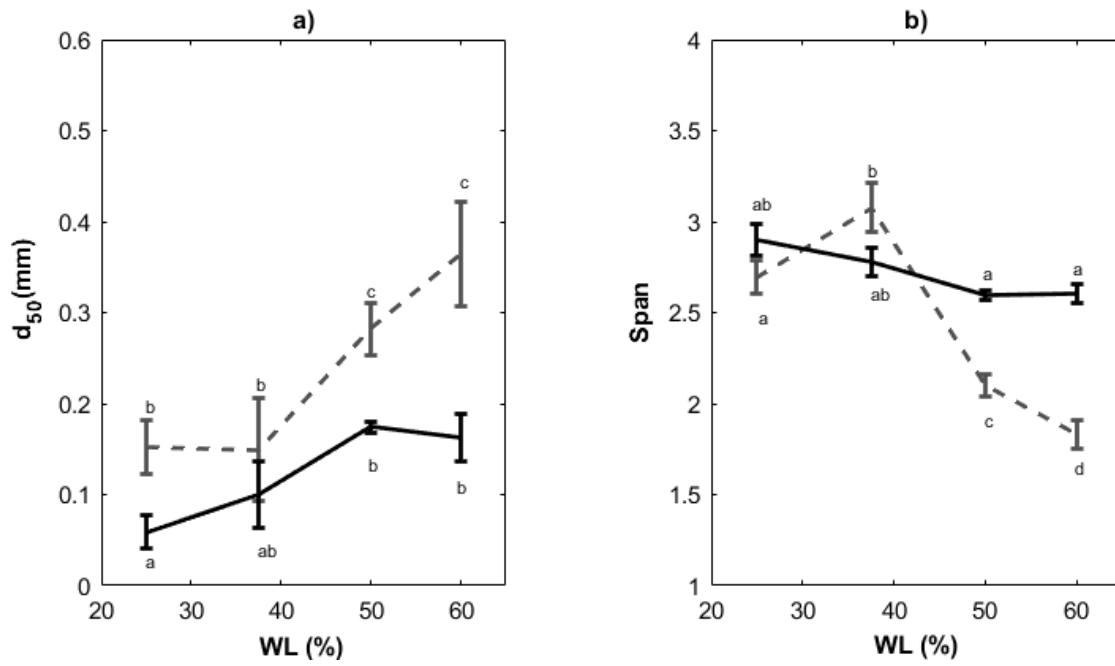


Figure 1: Evolution of the a) median diameter (d_{50}) and b) heterogeneity of the pore size distribution (span) in 1 mm of crust as a function of water loss for hot-air fries (---) and deep-fat fries (—). The marks with the same superscript (a–d) do not differ significantly (Fisher LSD test, P value ≤ 0.05). Error bars represent the standard deviation between replicates.

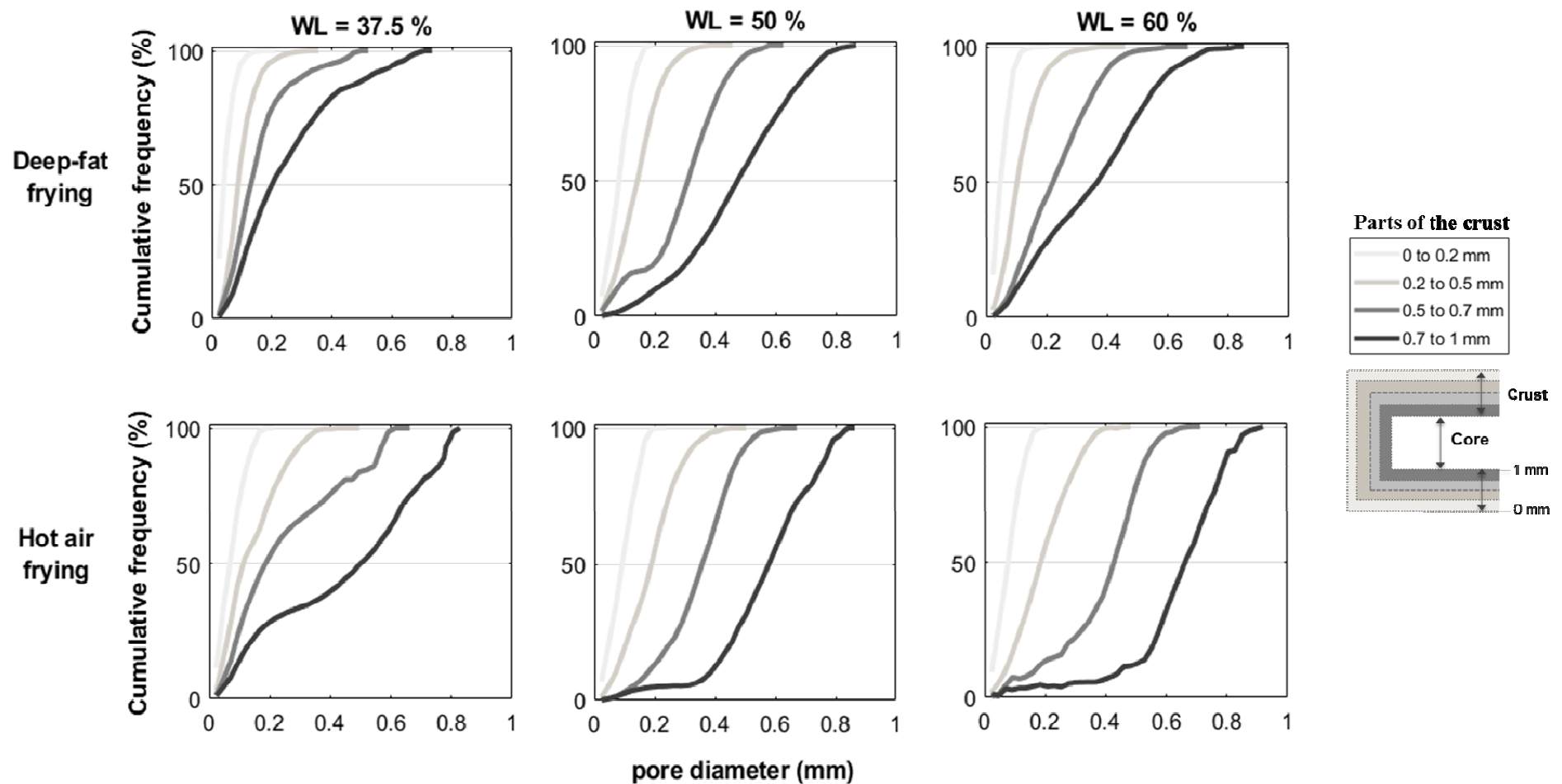


Figure 1: Pore diameter distribution in different parts of the crust during hot-air frying and deep-fat frying for different water loss (WL).

The pore diameter globally increases from the surface to the core of the fry for the same water loss. The pore size of the hot-air fries is larger than that of deep-fat fries in the different parts of the crust except for the first 0.2 mm.

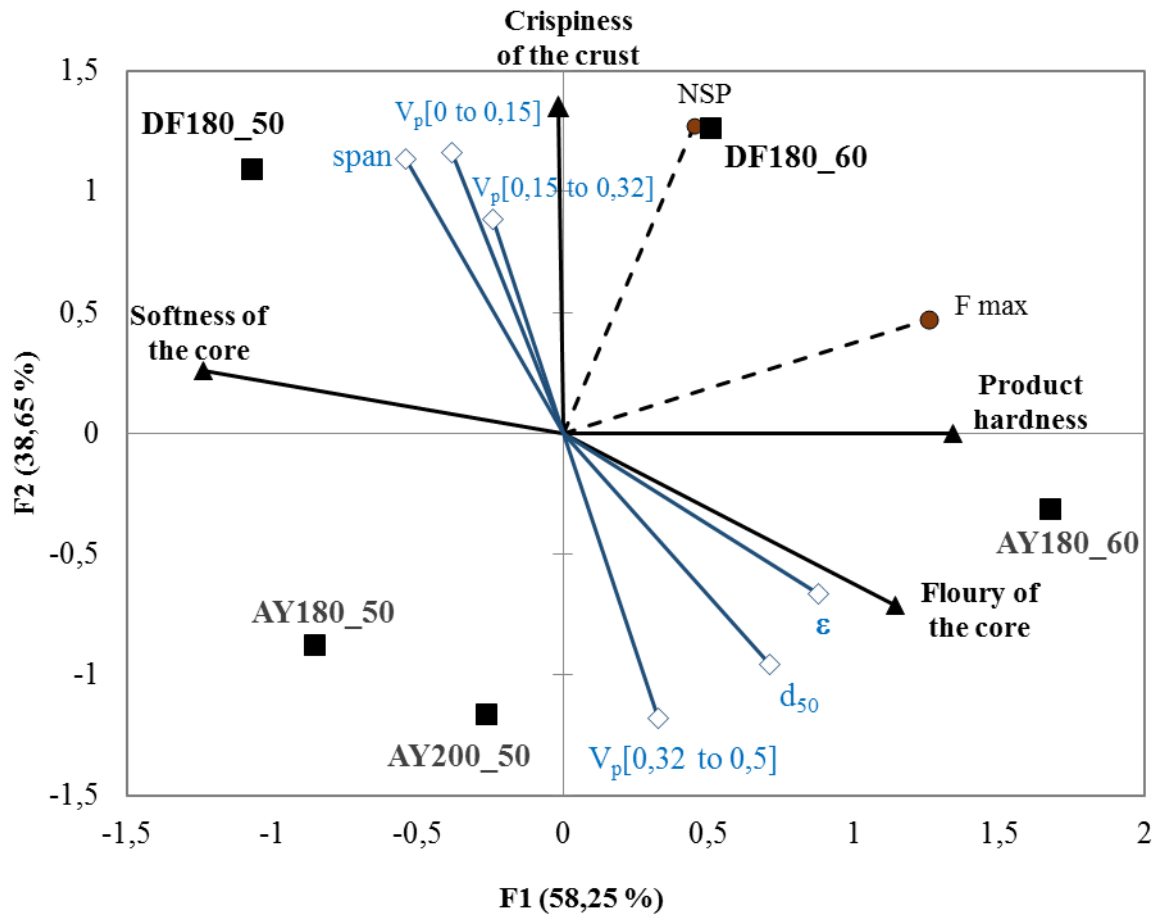


Figure 1: Bi-plot of PCA regarding sensory descriptors (▲) according to (Gouyo et al., 2019), instrumental data (●) according to (Gouyo et al., 2019) and microstructure parameter (□) dataset for French fry samples (■) obtained by deep-fat frying (DF) or air frying (AY) at different temperatures (180 and 200 °C) and different water loss levels of 50 and 60% (i.m.).

$V_p[0 \text{ to } 0,15]$ = volume of pores with diameter ranging from 0 to 0.15 mm.

$V_p[0,15 \text{ to } 0,32]$ = volume of pores with diameter ranging from 0.15 to 0.32 mm.

$V_p[0,32 \text{ to } 0,5]$ = volume of pores with diameter ranging from 0.32 to 0.5 mm.

ϵ = total porosity

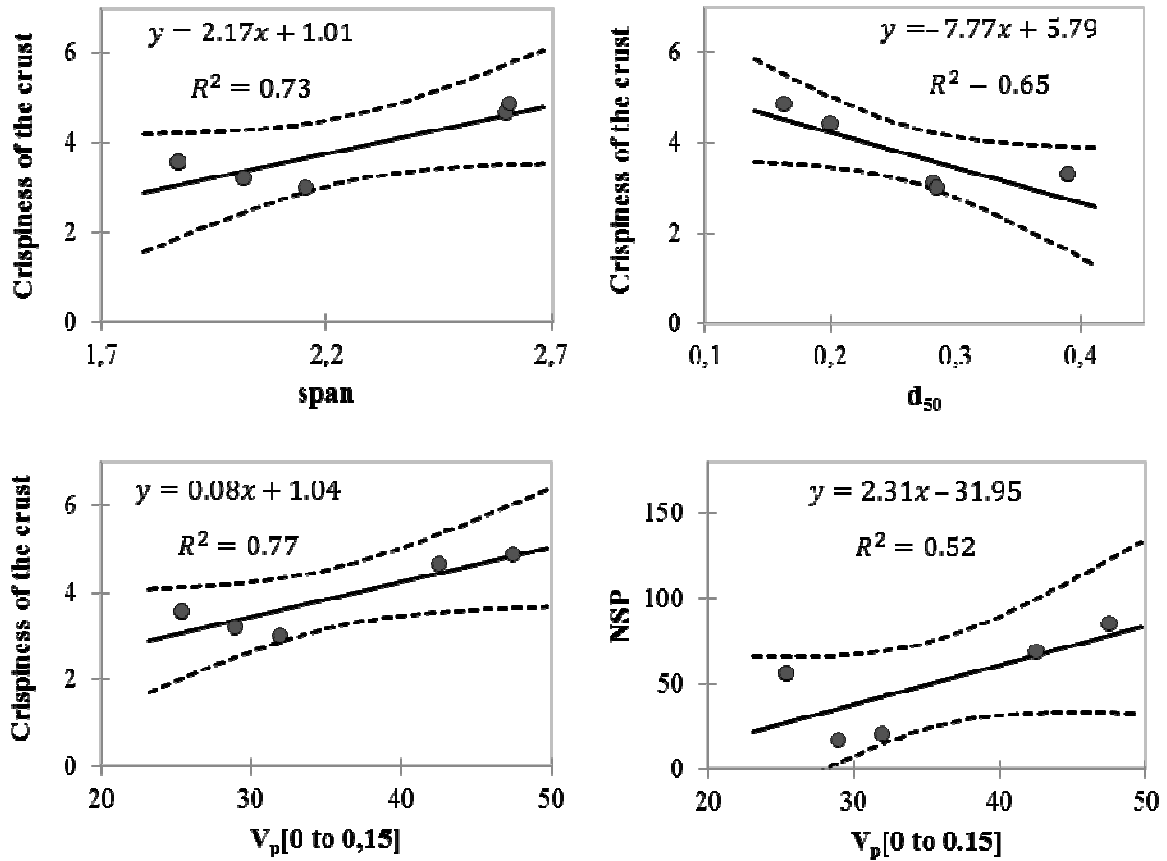


Figure 1: Linear regression (solid line) between sensory descriptors (y = crispness of the crust) and microstructure parameters (x = span, d_{50} and $V_p[0 \text{ to } 0,15]$) and between the number of sound peaks (y = NPS) and $x = V_p[0 \text{ to } 0,15]$. 95% confidence interval (dashed line). $V_p[0 \text{ to } 0,15]$ represents the volume of pores with diameter ranging from 0 to 0.15 mm.